A pediatric robotic thumb exoskeleton for at-home rehabilitation

The isolated orthosis for thumb actuation (IOTA)

Patrick Aubin
Rehabilitation and Development Center of Excellence for Limb Loss Prevention and Prosthetic Engineering, VA Puget Sound Health Care System, Seattle, Washington, USA
Kelsey Petersen, Hani Sallum and Conor Walsh
Wyss Institute for Biologically Inspired Engineering, Harvard University, Boston, Massachusetts, USA
Annette Correia
Boston Children's Hospital, Boston, Massachusetts, USA, and
Leia Stirling
Wyss Institute for Biologically Inspired Engineering, Harvard University, Boston, Massachusetts, USA and Massachusetts Institute of Technology, Cambridge, Massachusetts, USA

Received 9 October 2013
Revised 7 March 2014
11 March 2014
Accepted 22 March 2014

Abstract

Purpose – Pediatric disorders, such as cerebral palsy and stroke, can result in thumb-in-palm deformity greatly limiting hand function. This not only limits children's ability to perform activities of daily living but also limits important motor skill development. Specifically, the isolated orthosis for thumb actuation (IOTA) is 2 degrees of freedom (DOF) thumb exoskeleton that can actuate the carpometacarpal (CMC) and metacarpophalangeal (MCP) joints through ranges of motion required for activities of daily living. The paper aims to discuss these issues.

Design/methodology/approach – IOTA consists of a lightweight hand-mounted mechanism that can be secured and aligned to individual wearers. The mechanism is actuated via flexible cables that connect to a portable control box. Embedded encoders and bend sensors monitor the 2 DOF of the thumb and flexion/extension of the wrist. A linear force characterization was performed to test the mechanical efficiency of the cable-drive transmission and the output torque at the exoskeletal CMC and MCP joints was measured.

Findings – Using this platform, a number of control modes can be implemented that will enable the device to be controlled by a patient to assist with opposition grasp and fine motor control. Linear force and torque studies showed a maximum efficiency of 44 percent, resulting in a torque of 2.39 ± 1.06 in.-lbf and 0.69 ± 0.31 in.-lbf at the CMC and MCP joints, respectively.

Practical implications – The authors envision this at-home device augmenting the current in-clinic and at-home therapy, enabling telerehabilitation protocols.

Originality/value – This paper presents the design and characterization of a novel device specifically designed for pediatric grasp telerehabilitation to facilitate improved functionality and somatosensory learning.

This work was funded by the Wyss Institute for Biologically Inspired Engineering at Harvard University and the Deborah Munroe Noonan Memorial Research Fund. The authors would like to thank Alessandro Puiatti for the helpful comments during the preparation of the manuscript.

International Journal of Intelligent Computing and Cybernetics
Vol. 7 No. 3, 2014
pp. 233-252

1756-378X
DOI 10.1108/IJICC-10-2013-0043

Keywords Pediatric, Exoskeleton, At-home hand rehabilitation, Rehabilitation robotics, Thumb
Paper type Research paper

1. Introduction

The human hand is a sophisticated instrument used to perform many activities of daily living. The opposable thumb is a remarkable anatomical feature of the hand which greatly increases the hand's versatility. Thumb opposition involves flexion, abduction, and medial rotation so that the pulp surface can contact the other digits (Jones, 2006). A variety of pediatric diseases and brain injuries can affect hand function, including cerebral palsy (CP), pediatric stoke, and traumatic brain injury. CP is the most common motor disability in children, affecting approximately 3.6 per 1,000 school-age children (Yeargin-Allsopp *et al.*, 2008). Approximately 47 percent of patients with CP have a thumb in palm deformity in at least one of their hands, which negatively affects hand function (Park *et al.*, 2011). According to the House classification, type II thumb-in-palm deformity is defined as fixed adduction of the carpometacarpal (CMC) joint and flexion of the metacarpophalangeal (MCP) joint (Damiano, 2006).

The goal of pediatric hand rehabilitation is to promote the independence of the patient by improving motor function. Depending on the severity, treatment can include stretching, serial casting, orthotic devices, chemical denervation, surgical release, and other techniques to help maintain range of motion and tone control in the upper extremity. All of these interventions require occupational therapy, which include the use of functional tasks within the treatment sessions and at-home exercise programs, to maximize function. Improvements in motor performance over time are due to neuroplasticity, which is enhanced in children, allowing the brain to reorganize neuronal networks and recover from brain damage (Johnston, 2009). Motor learning strategies that incorporate massed practice, cognitive engagement, and functional relevance are considered essential to successful therapy for pediatric movement disorders (Damiano, 2006).

Rehabilitative programs that can be performed at home have the potential to augment standard care and have the advantage of being more convenient, less expensive, and provide greater training frequency and intensity than conventional care delivered one-on-one by a therapist in a clinic. Robotic rehabilitation devices can be programmed to apply precise motions or torques to relevant joints in a repetitive manner during active participation while quantitatively monitoring progress over timescales that range from seconds to months. Through the use of video games or interactive feedback, these robotic rehabilitation therapies can also be entertaining and motivating which may help maintain use and encourage the completion of a rehabilitation program.

Robotic rehabilitative devices for the hand can either be end-effector (Dovat *et al.*, 2008; Lambercy *et al.*, 2007; Kawasaki and Mouri, 2007) or exoskeleton (Schabowsky *et al.*, 2010; Loureiro and Harwin, 2007; Turner *et al.*, 1998; Bouzit *et al.*, 2002; Connelly *et al.*, 2009) based systems. End-effector systems, such as the cable actuated handcare (Dovat *et al.*, 2008), only constrain the distal phalanges of the fingers while the proximal joints are unconstrained. Thus, if explicit control of each joint is desired, an exoskeletal system rather than an end-effector system is necessary. Exoskeleton systems can simultaneously constrain distal and proximal joints such as the proximal inter-phalangeal joint and the metacarpal phalangeal joint. For exoskeleton based systems, the robotic super structure can be mounted either in the palmar region of the

hand as in Bouzit *et al.* (2002), or on the dorsum of the hand (Schabowsky *et al.*, 2010; Loureiro and Harwin, 2007; Turner *et al.*, 1998; Godfrey *et al.*, 2010). One limitation of devices with hardware in the palmar region is their inability for the user to perform palmar or pincer grasps, two functionally important motor control strategies, in real (not virtual reality) environments. Exoskeleton systems for the hand can have independent degrees of freedom (DOF) for each finger as in (Bouzit *et al.*, 2002; Connelly *et al.*, 2009) or they can lump the index through the small finger together into one functional unit with 1 DOF (Lambercy *et al.*, 2007; Schabowsky *et al.*, 2010; Loureiro and Harwin, 2007; Godfrey *et al.*, 2010; Ochoa *et al.*, 2009).

While the field of rehabilitation robotics has seen significant growth recently, very little work has been focussed on pediatric applications (Fasoli *et al.*, 2012). In particular, no pediatric exoskeleton systems have been developed for hand rehabilitation. Such a device requires particularly careful design in terms of both its anthropometric size and weight; a system designed for an adult cannot simply be scaled down in size. Also, its user interface must be simple enough for a child to use. In addition, few studies have investigated the usability of at-home robotic rehabilitation devices or the feasibility of integrating rehabilitation robotics into a home therapy program. Given the incidence of pediatric stroke, traumatic brain injury, CP, and other disorders, it follows that a pediatric robotic rehabilitation system for the clinic and home would be highly beneficial.

The long-term goal of this research is to determine the effectiveness of robot-assisted therapy to augment pediatric motor learning and recovery using a wearable robotic orthosis. The opposable thumb is critical for grasping and manipulating objects and is responsible for 40 percent of hand function (Carlson *et al.*, 2006). For this reason we focussed first on developing a system that assists and rehabilitates the thumb, specifically the CMC and MCP joints, which are required for opposition grasp.

The aim of this paper is to present the design specifications, electrical and mechanical components, linear force and joint torque characteristics, and control methodologies for an isolated orthosis for thumb actuation (IOTA). IOTA (Figure 1) is a pediatric robotic thumb exoskeleton for at-home rehabilitation. Unlike many traditional exoskeletons, the IOTA device was designed specifically for children between the ages of eight and 12 to facilitate actuation of the CMC and MCP joints of the thumb. The device was designed to be used within a home setting while performing natural tasks, making portability, and ease of use paramount design considerations. In addition, IOTA does not obstruct the palmar region of the hand so it has the potential to be used during everyday activities, thus extending usage beyond virtual reality environments.

2. Device specifications

The mean adult flexion-extension range of motion of the CMC and MCP joints have been reported to be 52.9° (Cooney *et al.*, 1981) and 110° (Yoshida *et al.*, 2003), respectively. The CMC has a mean adduction-abduction range of motion of 42.4° (Cooney *et al.*, 1981) while the MCP functions mostly as a flexion-extension hinge joint (Yoshida *et al.*, 2003) (Figure 2). From these data and from professional experience, 60° of rotation for the CMC and MCP joints was assumed to be a reasonable functional range of motion. Here we restrict CMC range of motion to only permit palmar abduction/adduction, thus restricting the ability to perform circumduction. Anthropometric sizing for the device was determined through pediatric databases (Snyder *et al.*, 1977). Our key measures of interest from the pediatric population were

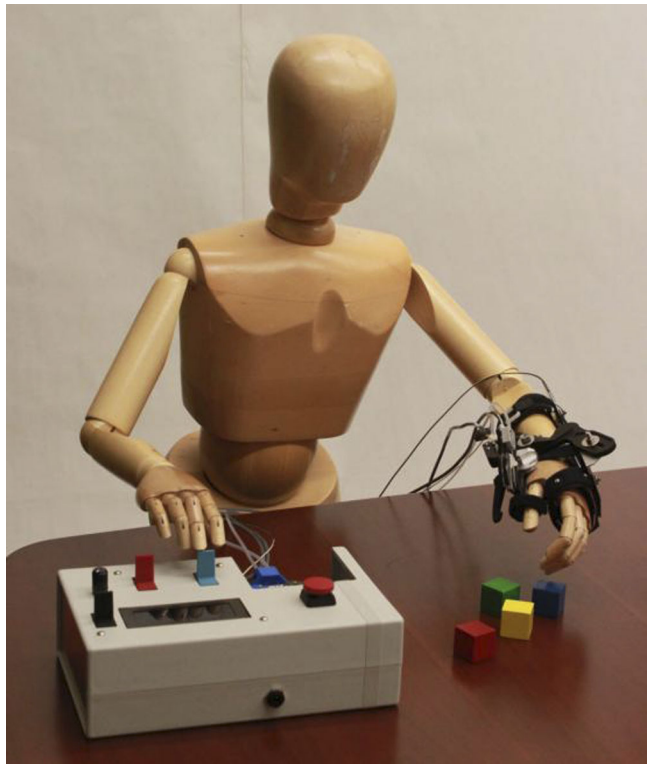

Figure 1.
The Isolated Orthosis for Thumb Actuation (IOTA) is a 2-DOF exoskeleton for clinical and at home pediatric thumb rehabilitation

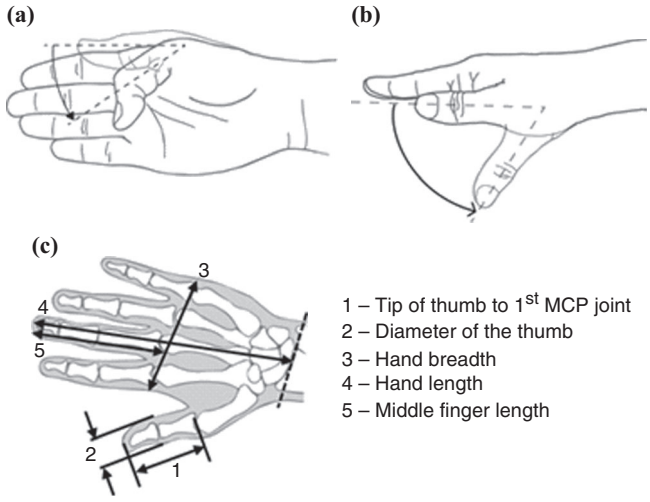

Source: Adapted from Hoppenfeld and Hutton (1976)

Figure 2.
A diagram of (a) flexion of the metacarpophalangeal (MCP) joint; (b) abduction of the carpometacarpal (CMC) joint; and (c) the anthropometric measures of the thumb

the thumb length, the thumb diameter, the palm length, and the hand breadth (Figure 2 and Table I). From these data, the IOTA was designed to allow the above stated 60° of CMC and MCP range of motion and fit children aged eight to 12 with the anthropometric measures of Table I.

A recent study performed by the authors examined the torque needed to passively abduct the thumb at the CMC joint in children with a diagnosis of hemiplegia or stroke. In this study, a passive modified wrist orthosis was fabricated with an adjustable thumb joint which could be placed over the CMC joint. The torque required to maximally abduct the thumb was recorded with a torque sensor. Preliminary results from this study indicated that the maximum and mean applied torques to reach maximum abduction in the affected side were $0.486\,\mathrm{N \cdot m}$ and $0.164 \pm 0.097\,\mathrm{N \cdot m}$. These data were used to specify the torque requirements for the IOTA system (Table I).

IOTA was designed to be lightweight so that children could wear the device while performing standard daily activities without being cumbersome. The target weight to be worn on the hand was specified to be $< 0.450\,\mathrm{kg}$ (approximately 40 percent of the combined weight of a seven year old child's hand, forearm and arm) (Table I). In order to facilitate use in a home setting, the device was specified to be compact, lightweight, and portable so that it could be easily carried by a parent and be deployable on a home table or desk (Figure 1). The initial design allowed for a control box on a table, with the intent to minimize the electronics in future versions so that the control box could be mounted to an arm or waist belt.

3. Electromechanical design and implementation

3.1 Mechanical design

The actuated orthotic component of the IOTA is composed of two parts; a semi-disposable patient-specific glove and a robotic exoskeleton that mounts to the glove. The glove is fitted to an individual subject's hand, and the exoskeleton can be adjusted to fit the full range of hand sizes specified (Figure 3). The glove is made of lycra fabric, delrin, and annealed aluminum alloy 1100 which is covered with a thin layer of soft neoprene rubber. The 1100 alloy aluminum is soft enough to be manually molded to the dorsum of an individual's hand by a therapist and has a flexible tab that extends around the first metacarpal toward the palm to secure the dorsal plate to the hand.

Characteristic	Requirement	
	Target	Actual
CMC range of motion	60°	67°
MCP range of motion	60°	67°
Hand mounted weight (kg)	0.45	0.23
Control box size	Table top	25.0 × 15.8 × 7.5 cm
Portability	Carried by one hand	Fits into brief case
Battery life (min)	45	> 160
Fit thumb lengths (cm)	4.0-6.4	4.0-6.4
Fit thumb diameters (mm)	14-16	10-16
Fit hand breadths	5.7-8.1	4.4-8.1
Fit children aged	8-12	8-12
Maximum torque for abduction (N · m)	0.486	0.384
Mean torque for max abduction (N · m)	0.164	0.103-0.384[a]

Note: [a]The available torque at maximum abduction will depend on the patient specific range of motion

Table I.
IOTA device specifications

A 0.75 mm delrin sheet extends from the aluminum dorsal plate proximally over the wrist and forearm and is secured with a Velcro strap proximal to the head of the ulna. The glove provides a stable base from which the exoskeleton can exert forces on the thumb, while allowing the subject to retain significant flexibility of the wrist and fingers (Figures 3 and 4). The delrin forearm plate also houses a 0.22 mm thick × 5.08 cm long bend sensor (Flexpoint Sensor Systems Inc., Draper, UT, USA) which extends across the wrist joint to measure flexion/extension (Figure 4). Measurement of wrist flexion/extension allows the device to simulate the tenodesis effect whereby wrist extension adducts the CMC and flexes the MCP joint and wrist flexion abducts CMC and extends MCP.

In order to minimize the weight on the subject's hand, the actuators for the CMC and MCP joints are located off-board of the orthotic and reside inside the control box. Actuation of the joints is achieved by two servos and two spring-return cable transmissions that connect to the orthotic. To actuate the CMC and MCP joints, the servos use internal encoders to determine servo angle. Optical encoders integrated

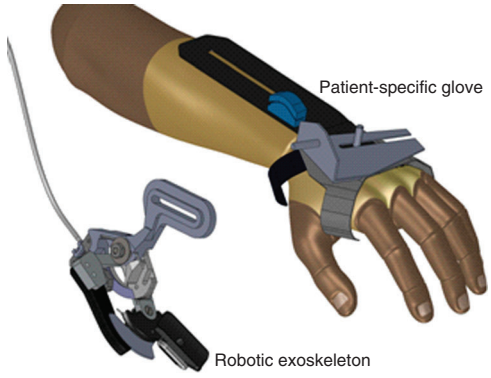

Figure 3.
A CAD rendering of the hand mounted components of the IOTA system including the actuated robotic thumb exoskeleton and a patient-specific dorsal glove

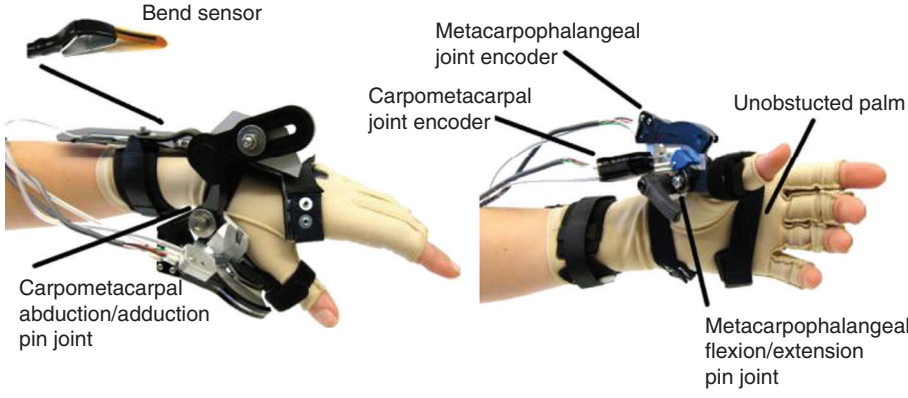

Figure 4.
The aluminum and delrin on the dorsal glove provide a stable platform to which the exoskeleton device is mounted and houses a bend sensor used to measure wrist flexion/extension

Notes: The exoskeleton has pin joints for the carpometacarpal and metacarpophalangeal joints and two encoders to measure angular rotation about those two joints. The degree of CMC circumduction can be set by an Occupational Therapist by the molded configuration of the aluminum

into the exoskeleton provide additional direct measurement of the CMC and MCP joint angles as well as estimations of cable position. The cable transmissions, sensor power supplies, and sensor signals are connected to the orthotic from the control box via a wire bundle (Figure 4).

3.2 Electromechanical design

An Arduino Mega 2560 (http://arduino.cc) was chosen as the microcontroller for the IOTA. A Cytron G15 shield (Cytron Technologies Sdn., Johor, Malaysia) is used with the Arduino board and controls the servo motors via half duplex serial communication. Dynamixel AX-12A servo motors (Robotis Inc., Seoul, Korea) were selected as they met the torque, speed, size, and weight requirements for the given application. The Dynamixel servos are connected in a daisy chain fashion and controlled by the serial packets sent from the Cytron shield via the communication bus. Each AX-12A servo has an internal angular position sensor with a resolution of 0.29° (300°/1,024 levels) (Figure 5).

The integrated wrist bend sensor changes resistance with sensor curvature. The bend sensor is connected to a voltage divider circuit with a potentiometer tuned to its base resistance. A two stage operational amplifier (Op-amp) with an adjustable gain ranging from 1.0 to 10.0 is used to amplify the output of the voltage divider circuit. The bend sensor produces a change in resistance of approximately 125 /°. The output

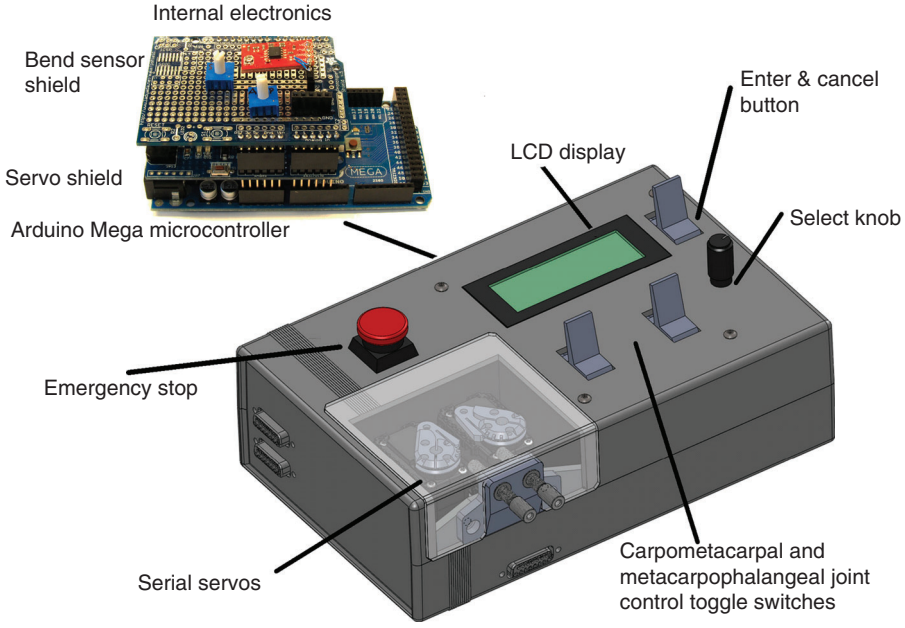

Figure 5.
The portable control box measuring 25.0 cm × 15.8 cm × 7.5 cm houses the Arduino Mega microcontroller board and servos

Notes: Momentary toggle switches, a knob and a 4x20 LCD display allow the user to control the exoskeleton joints and navigate through the different IOTA modes of operation. The Arduino Mega 2560 microcontroller based board connects to a Cytron G15 serov shield which communicates with the Dyamixel AX12-A servo motors via a half-duplex single line serial protocol. The servos have internal potentiometer position sensors

of the Op-amp circuit is connected to the ten-bit A/D converter on the Arduino Mega and is proportional to wrist flexion/extension angle (Figure 6).

Three momentary toggle switches and a rotary knob on the control box are used to navigate through a menu system for setting the appropriate control modes and therapy routines and for manual control of the exoskeleton. The function of the buttons changes depending on the mode of operation. A 4 × 20 LCD presents the navigable menu system to the user and displays messages and instructions when necessary. An emergency stop button immediately halts servo motion if pressed (Figures 1, 5, and 6).

3.3 Control system design

Immediately after turning on the device, a calibration protocol is performed to set user-dependent safety limits for the CMC and MCP range of motion and to obtain the wrist range of motion. When the child is with the therapist, the interaction with the device is performed as a collaboration between the child and therapist, with level of child interaction depending on the child's age and attentional resources. In an at-home setting, the calibration would be performed by a parent in collaboration with a child. Operationally, a parent would be trained on how to use the device with the therapist prior to having a device available in the home environment. This strategy is common with pediatric medical devices. To set the CMC and MCP range of motion limits, the adult-child team uses the toggle switches to manually actuate the CMC and MCP joints to the maximally adducted and flexed position, respectively, and then into a maximally abducted and extended position. The thumb, index, and pinky fingers are color coded on the exoskeletal glove to match the calibration instruction sheet, which shows pictures of the calibration positions to simplify this task for the child. For example, to depict the motion toward the adducted and flexed position the instruction sheet shows the thumb (colored blue) moving toward the index and pinky fingers (in green and red, respectively). These colors also match the toggle switches, where green represents CMC motion toward and away from the index finger and red represents MCP motion toward and away from the pinky. The CMC and MCP angles achieved during this procedure are stored in the device as the range of motion limits. The wrist range of motion is then recorded by asking the participant to perform a maximally flexed and then maximally extended wrist motion. After the calibration procedure is completed the user can select one of the control modes.

We initially developed four controllers that provided differing levels of direct user interaction – manual control (manual mode), automated motion assist (cyclic mode with teach and learn mode), and two controllers that provided a kinematic based user-activated motion (wrist control mode and functional assist mode). In the development of the first set of controllers, we specifically excluded user intent decision

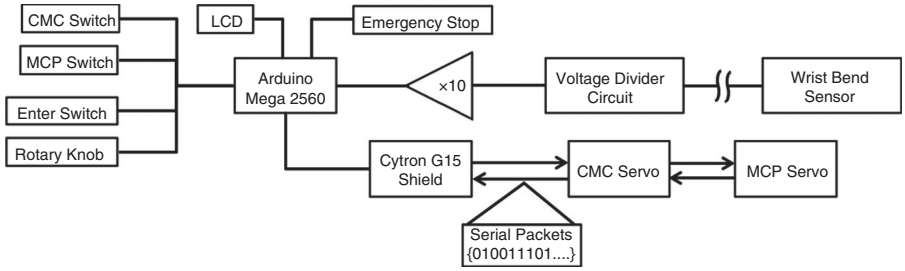

Figure 6.
Schematic of the electromechanical system depicting data flow of the wrist bend sensor, Dynamixel AX-12A servo motors, and navigation subsystems

making via neural or muscular signals. However, these techniques are currently an area of active investigation (e.g. electromyography signals include: Saponas *et al.*, 2008); Khokhar *et al.*, 2010); Micera *et al.*, 2010; Ambrosini *et al.*, 2011; and electroencephalography signals include: Tillery *et al.*, 2003; Broetz *et al.*, 2010; Ortner *et al.*, 2011). While these methods have great potential for an exoskeleton control framework that may require lower mental loads on the user, there is still significant work to be done on developing these electrophysiological signal techniques such that they are robust enough in an at-home setting for functionally relevant tasks in a pediatric population. Thus, the controllers initially integrated permit the evaluation of system interaction using robust kinematic sensing and would allow at-home testing for functionally relevant tasks in an initial pilot study. The following subsections describe these control modes.

3.3.1 Manual control mode. In manual control mode, the toggle switches located below the LCD screen on the control box are used to flex/extend and adduct/abduct the MCP and CMC joints. The joints can be actuated individually or simultaneously. The speed of actuation (°/s) is set by the user's selection of slow, medium, or fast and is controlled by a built-in speed control loop in the servo. If the user tries to manually actuate the CMC or MCP joint to a position beyond the specified range of motion limit the software will stop the servo motors to prevent injury to the user.

3.3.2 Teach and learn mode. The purpose of the teach and learn mode is to record therapist-assisted thumb motion for later playback. Here the occupational therapist manually moves a patient's thumb through a range of motion while the patient is wearing the exoskeleton. For the therapist to manipulate the thumb freely, the device must be as mechanically transparent to the wearer as possible. This means the servo motors must respond to motions generated by the therapist to permit an appropriate cable tension (Figure 7). Insufficient cable slack prevents motion and too much slack may cause the cable to become dislodged from its guide, thus disrupting the transmission of torque to the exoskeletal joint. This scheme can be thought of as a

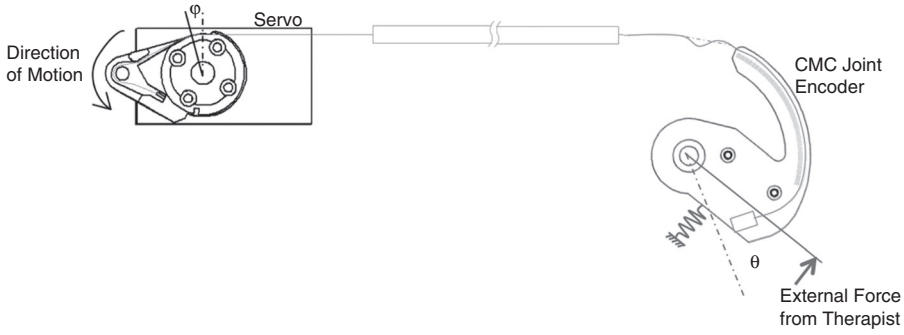

Figure 7.
Gross system motion is shown for the CMC joint in two different stages, no external force represented by dashed lines and a thumb extension force shown with solid lines

Notes: With no external force the cabling is relaxed and no servo motion is necessary for slack compensation. When an external joint displacement (flexion or extension) occurs, the encoder alerts the system that the amount of slack has changed. The servo motor then compensates for this change in slack amount by increasing or decreasing its angular position in turn adjusting the available cable length which facilitates movement to the desired joint position

cable slack regulator, whereby a proportional controller is used to maintain a specified length of cable slack in the cable driven joints. If the patient's thumb is moved by the therapist so as to tighten the cable, then the servo will rotate to loosen the cable. Similarly, if the patient's thumb is moved so as to loosen the cable, as seen in Figure 7, then the servo will rotate to compensate for the additional slack and tension the cable system. The system follows the joint motion imposed by the therapist by maintaining a fixed small amount of slack, corresponding to a 10° difference between servo and joint angular positions, within each joint. These internal positions are updated every 200 milliseconds to respond to therapist motion. A proportional controller regulates the cable slack by monitoring the difference (δ) between the MCP and CMC servo angular positions ($\varphi_{MCP}{}^{\circ}$ and $\varphi_{CMC}{}^{\circ}$), as measured by the servo encoders, and the MCP and CMC joint positions (θ_{MCP} and θ_{CMC}), as measured by the joint encoders, Equations (1) and (2):

$$\delta_{MCP} = \varphi_{MCP} - \theta_{MCP}, \tag{1}$$

$$\delta_{CMC} = \varphi_{CMC} - \theta_{CMC}. \tag{2}$$

If δ_{MCP} (or δ_{CMC}) is greater than a small positive threshold ($d_1{}^{\circ}$) then the therapist has applied a flexion force on the patient's thumb in a manner so as to decreased θ_{MCP} (or θ_{CMC}) and the servo should rotate to decrease φ_{MCP} (or φ_{CMC}). If δ_{MCP} (or δ_{CMC}) is less than a small negative threshold ($-d_1{}^{\circ}$) then the therapist is applying an extension force on the patient's thumb in a manner so as to increase θ_{MCP} (or θ_{CMC}) and the servo should rotate to increase φ_{MCP} (or φ_{CMC}) (Figures 7 and 8). After manipulation, the maximum and minimum MCP and CMC joint angles are recorded and saved for later playback within the cyclic control mode. The new maximum and minimum angles can be related to therapy exercises or functional tasks, for example twisting off different sized caps from drinking bottles, in which having a singular calibrated maximum or minimum would be limiting. Future implementations may save the joint trajectories for more complex motions.

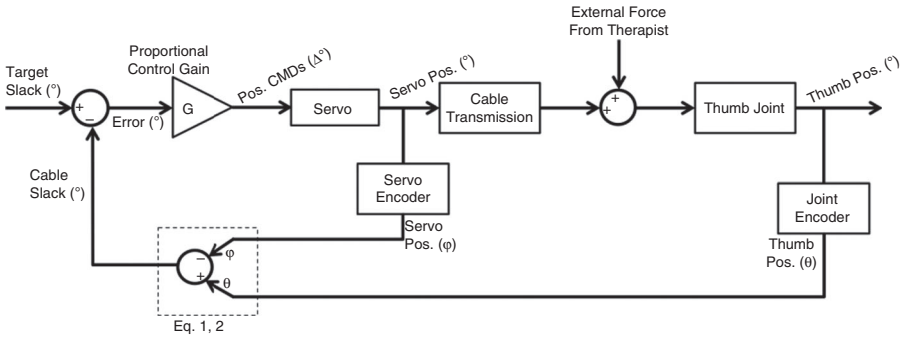

Figure 8.
A cable slack regulator with proportional feedback control is used to make the exoskeleton sytem mechanically transparent during the teach and learn mode

Notes: A constant amount of slack is maintained on the transmission cable by comparing the servo position to the thumb joint positions. The error signal between the target slack and the actual slack is sent as a delta position command to the servo motors. The system updates every 200 miliseconds in order to track and respond to the motion of the therapist

3.3.3 Cyclic control mode. Cyclic control mode allows a pre-set trajectory for the CMC and MCP joints to be repeated a set number of times. The nominal trajectory moves the CMC and MCP joints through their full range of motion. The joints are actuated simultaneously at a speed of slow, medium, or fast as specified by the user until they reach their range of motion limit and then they are actuated in the opposite direction until the other end range of motion is reached. This cycle is then repeated a certain number of times based on the user selection. Additional trajectories can be created using teach and learn mode and implemented in cyclic control mode.

3.3.4 Wrist control mode. Wrist control mode utilizes the bend sensor mounted across the wrist to provide a signal that can modulate the CMC and MCP thumb joint angles. In healthy individuals, as the wrist is moved from flexion to extension, there is a natural synergy called the tenodesis effect that causes finger flexion (Su *et al.*, 2005). Patients with poor grasp control often exploit the tenodesis effect by extending their wrist when they need assistance with finger flexion; thus we believe such a control strategy will be intuitive for them. As the wrist is flexed the servo motors actuate so as to extend the MCP and abduct the CMC. Similarly, if the user extends her or his wrist then the IOTA will actuate to flex the MCP and adduct the CMC. In all cases the CMC and MCP joints are actuated at a constant speed specified by the user until a range of motion limit is reached.

3.3.5 Functional assistance mode. The functional assistance mode seeks to anticipate the desired motion of the user and then assists with that motion. The target patient population for this system typically has some volitional control of their thumb but lacks the necessary strength or persistent coordination to perform functionally useful tasks. In this scenario, the functional assistance mode will be helpful as it augments the volitional motion. Thus, a small initial motion by the user generates a larger response motion. In the functional assistance mode the system continuously monitors the orientation of the patient's thumb. If the patient performs a small weak MCP extension, greater than a minimum threshold value and either maintains that position or begins flexion, the servos will actuate the MCP and CMC joints to the maximum range of motion. Once the MCP and CMC joints are rotated to their maximum positions they are held there momentarily and then released back into their flexed and adducted poses. This hold time is configurable by the user. This mode permits adaptation with recovery, as the minimum threshold can be modified to encourage additional motion prior to assistance. Further, assistance is only provided when the user no longer can attain increased MCP extension. Thus, if the user is able to perform the motion, the system will not provide assistance.

4. Device characterization

When evaluating how a device can improve patient functionality, it is important to first have a quantitative understanding of the system capabilities. If system efficacy is not observed, these data then permit the ability to distinguish if this may be due to a hardware issue (requirement of larger forces) or a controller issue (forces are sufficient, but perhaps they are not provided appropriately). For these characterizations, we specifically focus on measurements of force and torque, assuming that movements are slow.

The selection of a cable driven system permitted the IOTA to have minimal mass on the hand, while still using off-the-shelf servo motor actuators. The cable-drive transmission consists of stranded wire surrounded by a protective tubing, which interact to generate frictional losses. The efficiency of the transmission determines the output torque at the exoskeletal joints that can assist the wearer. To quantify these

transmission losses, and thus system efficiency, a linear force measurement was performed with a Futek load cell (Futek Inc., Irvine, CA; model No. FSH00103) and IHH500 measurement device (model No. FSH03571). We evaluated the effect of transmission length and overall orientation (i.e. straight, coiled, or twisted) as both contribute to reduced maximum output force in the system. Three different orientation configurations were used to characterize the effect of transmission orientation, which are relevant for clinical operational use.

In addition to the cable transmission losses characterized through the linear force testing, there is also the possibility of additional mechanical losses in the system. Thus, experiments were performed to measure the direct torque applied to the MCP and CMC joints for a range of joint orientations. As the torsional spring should have a linear response in the device operational region, it was hypothesized that torque measurements would be similar between joint orientations for each joint.

4.1 Linear force characterization

4.1.1 Methodology. The expected output torque of an AX-12A servo driven at the IOTA system voltage of 7.4 V is approximately 1.18 N · m (Robotis Dynamixel AX-12 User's Manual). For this characterization, a Futek load cell with a maximum measurement capacity of 22.2 N was used to measure the force at the end of different cable transmission lengths and orientations. A custom servo cable horn (with moment arm of 0.064 m) was designed for characterization so that the maximum expected output force of 18.51 N could be measured. The standard IOTA horn (with moment arm of 0.011 m) would have generated a maximum expected output force of 107.27 N.

The test rig for this experiment was designed to accommodate all transmission cable configurations (Figure 9). The IOTA system and transmission cable made up one end of the test rig. At the other end of the rig, the Futek load cell was mounted to 80-20 construction rails and a wire adapter to measure forces in tension. These test rig ends were designed so that the attachment points were collinear, thus preventing any off axis loading error during testing. A second adapter was created to hold the tubing

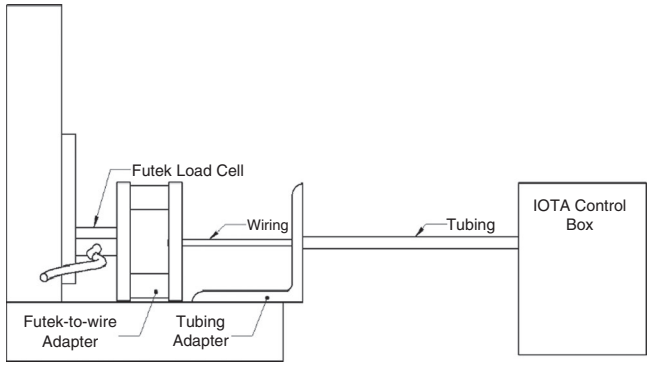

Figure 9.
The linear force test was comprised of a Futek load cell, a Futek-to-wire adapter fixture, a tubing holder, and the IOTA control box

Notes: The Futek-to-wire adapter allows for the wiring to be attached to the Futek for measurement. Both the Futek-to-wire and tubing adapter decrease off-axis loading error in the system. Wire lengths were taken as the distance from the Futek-to-wire adapter to the control box

making the test rig resemble the cable layout between the control box and the exoskeleton of the IOTA system. This design allows the cable to freely move throughout the fixed tubing. Using this system, we tested lengths of 2 in., 3, 5, 10, and 15 ft (0.05, 0.91, 1.52, 3.05, and 4.57 m) in straight-lined, coiled, and twisted positions. A coiled position was defined as having a 4 in. (0.10 m) diameter loop within an otherwise straight lined cable transmission. The twisted orientation was when one end of the test rig was horizontally turned clockwise four times before testing commenced, creating twists within the cable.

Data were recorded using the Futek load cell and measurement device with Futek Sensit software. For all testing combinations, eight trials were performed for 15 seconds each at a sampling rate of 10 Hz. Data were exported to Matlab (Mathworks, Natick, MA) for post-processing. The output variable of interest was the average sustained linear force of each trial for each testing configuration. Steady state was defined for each trial as when the data maintained a value within 5 percent of the mean linear force between the derivative's inflection points (Figure 10). Time to steady state was then defined as the first time after recording started that each data set reached this criterion. The mean of the force three seconds after steady state was reached was defined as the sustained linear force. Trials were then averaged together based on their length/position combination and a standard deviation between trials was performed.

4.1.2 Results. Summary of linear force testing results are provided in Table II. When operating at 7.4 V, the maximum sustained force exhibited by the system occurred at the shortest cable transmission length (2 in./0.05 m) and was 8.140 ± 0.623 N ($0.517\ \text{N} \cdot \text{m}$ for this configuration), which is a 44 percent efficiency from the available servo torque. When the orientation of the cable was straight, sustained linear force efficiency ranged from 13 to 44 percent. The coiled and twisted orientations were found

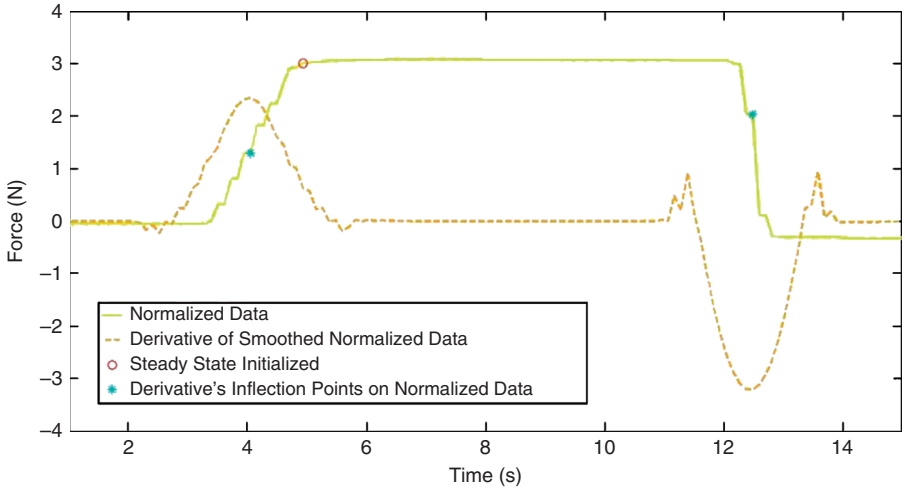

Notes: The point of steady state initialization was found by initially normalizing by the first three seconds of the data set then taking the derivative of that normalized data. The point at which an inflection point occurred in the derivative marked where averaging of the normalized data would begin and end. The point of steady state was then marked at the first occurrence where the data were within 5 percent of this average

Figure 10.
Sample of post-processed linear force characterization data

to have efficiencies ranging from 1 to 33 percent. The greatest losses were found for a 15 ft (4.57 m) length cable with a coiled orientation.

4.2 Joint torque characterization

4.2.1 Methodology. For this characterization, a MULTITORQ torque sensor (CDI Corp., Philadelphia, PA, model No. 101-I-MT) with a maximum measurement capacity of 1.130 N · m was used to measure the output torque applied at the CMC and MCP joints, individually. For these measurements, the nominal system design with a 5 ft (1.52 m) transmission cable was used. As the linear force characterization found this configuration generated 0.438 ± 0.022 N · m, no changes were needed to the nominal system for these characterization measurements with the sensor implemented.

The test rig for this experiment (Figure 11) was designed to hold the torque sensor's housing and the IOTA exoskeleton static while the torque sensor and exoskeletal joint were free to move. The torque sensor was mounted on one side of a 1-in. 80-20 construction rail while the exoskeleton was mounted on the other side. The rig required the design and 3D printing of connector "caps." These caps were designed to snap or screw onto the existing exoskeleton to permit usage of the torque sensor to measure

Table II.
Linear force study results

	2 in./0.05 m (N)	3 ft/0.91 m (N)	5 ft/1.52 m (N)	10 ft/3.05 m (N)	15 ft/4.57 m (N)
Straight	8.140 ± 0.623	5.211 ± 0.464	6.891 ± 0.340	2.407 ± 0.401	2.841 ± 0.241
1 Coil (4 in. diameter)	–	2.088 ± 0.154	3.064 ± 0.293	0.188 ± 0.157	0.129 ± 0.024
Twisted (4 twists)	–	3.524 ± 0.263	6.218 ± 0.130	2.637 ± 0.068	1.242 ± 0.621

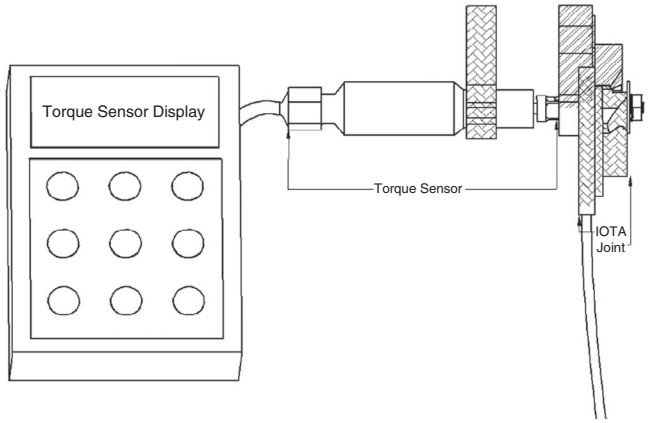

Figure 11.
The joint torque characterization used a torque sensor and a customized connection cap with a hole located directly over the exoskeletal joint where the sensor was inserted

Notes: The cross-hatched components of the figures denote pieces of the test rig which were mounted to a vertical 80-20 construction rail (not shown) to hold the components static during the experiment. These static portions ensured that the only torque being measured was at the IOTA joint. The diagonaled component marks the connection cap and joint pieces which were free to move to report a torque

the torque directly at the joint. The cap had a hole located over the joint where the torque sensor was inserted. Separate caps were designed for the CMC and MCP exoskeleton geometries.

The IOTA encoder reference frame defines a fully closed orientation as 0° and a fully open position as 67° (Figure 12). Note that closed is when the centerline of the cap geometry is parallel to the vertical 80-20 construction rail and open is denoted as 67° counterclockwise from the closed position. Five orientations across this range were selected for making measurements (0°, 17°, 33°, 50°, and 67°). The maximum torque was defined as the torque measured when the AX-12 motor stalled. The IOTA system actively assists opening but relies on a spring located at the exoskeletal joint for the closing motion. Thus, characterizations were obtained for the opening motion to understand the joint torque provided only by IOTA's motor assist. Eight trials were recorded for each orientation for both the CMC and MCP joints.

4.2.2 Results. Means and standard deviations were calculated for each orientation for the CMC and MCP joints (Table III). No torques were registered for measurements made at a starting position of 67° since the servo could not mechanically move any further, thus these values are not presented and are not included in the analysis. Separate Pearson product-moment correlation coefficients were computed in Matlab

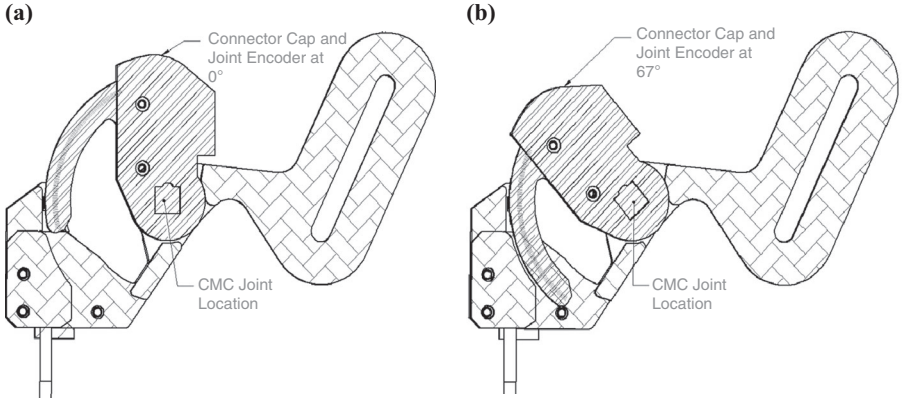

Notes: The cross-hatched component were held static during testing while the diagonaled component moved which allowed torque measurement to be taken for only the torque at the specified joint

Figure 12.
(a) Shows the CMC exoskeleton joint in a 0° fully closed position; and (b) shows that same joint moved into a 67° fully open position

	0° (N · m)	17° (N · m)	33° (N · m)	50°(N · m)	Overall average (N · m)
MCP	0.124 ± 0.006	0.083 ± 0.013	0.061 ± 0.008	0.043 ± 0.017	0.078 ± 0.005
CMC	0.384 ± 0.039	0.320 ± 0.031	0.273 ± 0.041	0.103 ± 0.013	0.270 ± 0.013

Note: Measurements were made from the most closed position (0°, 17°, 33°, or 50°) to an open position at 67°. Values are the presented as the mean and standard deviation of the measured torque

Table III.
Joint torque characterization summary

(Mathworks, Natick, MA) to assess the relationship between joint orientation and measured torque for the CMC and MCP. There was a negative correlation between the two variables for both the CMC ($r = -0.918$, $p < 0.001$) and MCP ($r = -0.921$, $p < 0.001$).

5. Discussion and future work

This paper presented the design specifications, electrical and mechanical components, linear force and joint torque characteristics, and initial control methodologies for the IOTA, an at-home grasping rehabilitation device for a pediatric population. The specifications for IOTA were based on pediatric anthropometric data so that children aged eight to 12 could use the device. The control modes for IOTA were designed to span simple specified movements to those that provide a kinematic user-activated assistance during grasping and object manipulation.

Through the characterization tests, we found that the IOTA system in the nominal configuration of 5 ft (1.52 m) straight cable had an efficiency of 37 percent with respect to the servo specifications. As would be expected, these efficiencies decreased when coils or twists were introduced into the cable transmission orientation. This highlights that when designing such systems care should be taken to ensure that cables are not overly constrained during operational use of the system.

We anticipated that the CMC and MCP torque would be largely independent of orientation since the magnitude of the servo output torque is large in comparison to the variation in the torsional spring torque. However, frictional losses in the transmission between the servos and the exoskeleton joints resulted in a significant negative correlation between the joint orientation and the measured torque. Thus the available torque when the hand is open is less than when the hand is closed. This is opposite of the previous human studies, which found that participants required greater torques when the CMC joint angle increased. In the nominal configuration, the device produced an average torque of $0.270 \pm 0.0.013\,\mathrm{N \cdot m}$ and $0.078 \pm 0.005\,\mathrm{N \cdot m}$ at the CMC and MCP joints, respectively. The maximum sustained torque that could be delivered was within 6 percent of maximum required torque found experimentally to passively reach thumb abduction by the study population and is able to provide the average torques found experimentally. The required system torques depend on the level of individual muscle contracture and the device presented here would meet the needs of the patients in this previous study.

While IOTA was specifically designed for House Class II patients, it could easily be adapted to other patients with increased muscle contractures by selecting larger actuators for the control box. As currently designed, the system is more appropriate for patients with limited control, as opposed to strong contractures. There are also several ways the system could be adapted to have the torque become more independent of exoskeleton joint orientation. One method would be to use a lower stiffness torsional spring with a greater preload.

In the long term, we aim to investigate the efficacy of an occupational therapy home exercise program based on a portable pediatric robotic system. To this end, we have an ongoing pilot study which aims to demonstrate that the IOTA can effectively facilitate a patient's ability to perform relevant functional evaluation tasks (i.e. box and block and nine-hole peg tasks) and demonstrate the ability to extend standard occupational therapy rehabilitation. Initial studies focus on functional measures of performance, while future studies will examine structural measures of rehabilitation.

6. Conclusion

The IOTA is an exoskeleton for assisting thumb motions in a pediatric population. The IOTA has the potential to provide increased freedom and independence for children with thumb-in-palm deformity. The device also has the potential to assist functionality and somatosensory learning, thus improving motor control without the device. We envision this device enhancing in-clinic and at-home therapy in addition to being a critical component of a telerehabilitation protocol for a pediatric population. In the current work, we addressed the design and test-bench evaluation of the IOTA. Future work will include device improvements (e.g. miniaturization of hardware and electronic components), integration of control algorithms relying on electrophysiological signals, and longitudinal human studies to evaluate functional rehabilitation and structural changes in the brain that occur with the use of robotic rehabilitation.

References

Ambrosini, E., Ferrante, S., Tibiletti, M., Schauer, T., Klauer, C., Ferrigno, G. and Pedrocchi, A. (2011), "An EMG-controlled neuroprosthesis for daily upper limb support: a preliminary study", *Conference Proceedings of the IEEE Engineering in Medicine and Biology Society*, pp. 4259-4262.

Bouzit, M., Burdea, G., Popescu, G. and Boian, R. (2002), "The Rutgers Master II-new design force-feedback glove", *IEEE/ASME Transactions on Mechatronics*, Vol. 7 No. 2, pp. 256-263.

Broetz, D., Braun, C., Weber, C., Soekadar, S., Caria, A. and Birbaumer, N. (2010), "Combination of brain-computer interface training and goal-directed physical therapy in chronic stroke: a case report", *Neurorehabilitation and Neural Repair*, Vol. 24 No. 7, pp. 674-679.

Carlson, M.G., Athwal, G.S. and Bueno, R.A. (2006), "Treatment of the wrist and hand in cerebral palsy", *The Journal of Hand Surgery*, Vol. 31A No. 3, pp. 483-490.

Connelly, L., Stoykov, M.E., Jia, Y., Toro, M.L., Kenyon, R.V and Kamper, D.G. (2009), "Use of a pneumatic glove for hand rehabilitation following stroke", *Annual International Conference of the IEEE Engineering in Medicine and Biology Society, IEEE Engineering in Medicine and Biology Society*, Vol. 2009 pp. 2434-2437.

Cooney, W., Lucca, M., Chao, E. and Linscheid, R. (1981), "The kinesiology of the thumb trapeziometacarpal joint", *The Journal of Bone and Joint Surgery American Volume*, Vol. 63 No. 9, pp. 1371-1381.

Damiano, D. (2006), "Activity, activity, activity: rethinking our physical therapy approach to cerebral palsy", *Physical Therapy*, Vol. 86 No. 11, pp. 1534-1540.

Dovat, L., Lambercy, O., Gassert, R., Maeder, T., Milner, T., Leong, T.C. and Burdet, E. (2008), "HandCARE: a cable-actuated rehabilitation system to train hand function after stroke", *IEEE Transactions on Neural and Rehabilitation Systems Engineering*, Vol. 16 No. 6, pp. 582-591.

Fasoli, S.E., Ladenheim, B., Mast, J. and Krebs, H.I. (2012), "New horizons for robot-assisted therapy in pediatrics", *American Journal of Physical Medicine & Rehabilitation/Association of Academic Physiatrists*, Vol. 91 No. 11, S3, pp. S280-S289.

Godfrey, S.B., Schabowsky, C.N., Holley, R.J. and Lum, P.S. (2010), "Hand function recovery in chronic stroke with HEXORR robotic training: a case series", *International Conference of the IEEE Engineering in Medicine and Biology Society*, Vol. 2010, pp. 4485-4488.

Hoppenfeld, S. and Hutton, R. (1976), *Physical Examination of the Spine and Extremities*, *Vol. 798*, Appleton-Century-Crofts, East Norwalk, CT.

Johnston, M.V. (2009), "Plasticity in the developing brain: implications for rehabilitation", *Developmental Disabilities Research Reviews*, Vol. 15 No. 2, pp. 94-101.

Jones, L. (2006), *Human Hand Function*, Oxford University Press, Oxford, New York, NY.

Kawasaki, H. and Mouri, T. (2007), "Design and control of five-fingered haptic interface opposite to human hand", *IEEE Transactions on Robotics*, Vol. 23 No. 5, pp. 909-918.

Khokhar, Z., Xiao, Z. and Menon, C. (2010), "Surface EMG pattern recognition for real-time control of a wrist exoskeleton", *Biomed Eng Online*, Vol. 9 No. 41, pp. 1-17.

Lambercy, O., Dovat, L., Gassert, R., Burdet, E., Teo, C.L. and Milner, T. (2007), "A haptic knob for rehabilitation of hand function", *IEEE Transactions on Neural Systems and Rehabilitation Engineering*, Vol. 15 No. 3, pp. 356-366.

Loureiro, R.C.V. and Harwin, W.S. (2007), "Reach & grasp therapy: design and control of a 9-DOF robotic neuro-rehabilitation system", *IEEE 10th International Conference on Rehabilitation Robotics*, pp. 757-763.

Micera, S., Carpaneto, J. and Raspopvic, S. (2010), "Control of hand prostheses using peripheral information", *IEEE Reviews in Bio-Medical Engineering*, Vol. 3, pp. 48-68, available at: http://ieeexplore.ieee.org/xpls/abs_all.jsp?arnumber=5598519

Ochoa, J., Dev Narasimhan, Y.J. and Kamper, D.G. (2009), "Development of a portable actuated orthotic glove to facilitate gross extension of the digits for therapeutic training after stroke", *The International Conference of IEEE Engineering in Medicine and Biology Society*, pp. 6918-6921.

Ortner, R., Allison, B., Korisek, G., Gaggl, H. and Pfurtscheller, G. (2011), "An SSVEP BCI to control a hand orthosis for persons with tetraplegia", *IEEE Transactions on Neural Systems and Rehabilitation Engineering*, Vol. 19 No. 1, pp. 1-5.

Park, E.S., Sim, E.G. and Rha, D.-W. (2011), "Effect of upper limb deformities on gross motor and upper limb functions in children with spastic cerebral palsy", *Research in Developmental Disabilities*, Vol. 32 No. 6, pp. 2389-2397.

Saponas, T., Tan, D., Morris, D. and Balakrishnan, R. (2008), "Demonstrating the feasibility of using forearm electromyography for muscle-computer interfaces", *CHI Conf Human Factors in Computing Systems, Florence, Italy, April 5-10*, AMC, New York, NY, pp. 515-524, available at: http://dl.acm.org/citation.cfm?id=1357138; http://dl.acm.org/citation.cfm?id=1357054&picked=prox&cfid=512848237&cftoken=63066552

Schabowsky, C.N., Godfrey, S.B., Holley, R.J. and Lum, P.S. (2010), "Development and pilot testing of HEXORR: hand EXOskeleton rehabilitation robot", *Journal of Neuroengineering and Rehabilitation*, Vol. 7 No. 36, pp. 1-17.

Snyder, R.G., Schineider, L.W., Owings, C.L., Reynolds, H.M., Golomb, D.H. and Schork, M.A. (1977), "Anthropometry of infants, children, and youths to age 18 for product safety design", Report No. UM-HSRI-77-17, Highway Safety Research Institute, The University of Michigan, Bethesda, MD.

Su, F.-C., Chou, Y.L., Yang, C.S., Lin, G.T. and An, K.N. (2005), "Movement of finger joints induced by synergistic wrist motion", *Clinical Biomechanics (Bristol, Avon)*, Vol. 20 No. 5, pp. 491-497.

Tillery, S., Taylor, D. and Schwartz, A. (2003), "The general utility of a neuroprosthetic device under direct cortical control", *Conference Proceedings of the 25th International Conference of IEEE Engineering in Medicine and Biology Society, Vol. 3, September 17-21*, pp. 2043-2046.

Turner, M., Gomez, D., Tremblay, M. and Cutkosky, M. (1998), "Preliminary tests of an arm-grounded haptic feedback device in telemanipulation", *Proceedings of the ASME IMECE Haptics Symposium, Vol. 1998*, pp. 1-6, available at: http://bdml.stanford.edu/oldweb/touch/publications/turner_asme98.pdf

Yeargin-Allsopp, M., Van Naarden Braun, K., Doernberg, N.S., Benedict, R.E., Kirby, R.S. and Durkin, M.S. (2008), "Prevalence of cerebral palsy in 8-year-old children in three areas of the United States in 2002: a multisite collaboration", *Pediatrics*, Vol. 121 No. 3, pp. 547-554.

Yoshida, R., House, H. and Patterson, R. (2003), "Motion and morphology of the thumb metacarpophalangeal joint", *The Journal of Hand Surgery*, Vol. 28 No. 5, pp. 753-757.

About the authors

Dr Patrick Aubin received the BS, MS, and PhD Degrees in Electrical Engineering from the University of Washington in 2004, 2006, and 2010, respectively. From 2012 to 2013 he was a Postdoctoral Fellow at the Wyss Institute for Biologically Inspired Engineering at Harvard University. Currently he is a Research Scientist at the Research, Rehabilitation and Development Center of Excellence for Limb Loss Prevention and Prosthetic Engineering at the VA Puget Sound Health Care System, Seattle, WA, USA. His research interests are in robotics, biomechanics, and rehabilitation.

Kelsey Petersen received a BS in Biomedical Engineering with a minor in Mechanical Engineering from the Boston University in 2013. She is currently a Postgraduate Research Fellow at the Wyss Institute for Biologically Inspired Engineering at Harvard University focussing on device design, prototyping, characterization, and clinical evaluation related to wearable devices. Her research interests include pediatric disorders, control systems, biomechanics, robotic rehabilitation, and neuroplasticity.

Hani Sallum received a BS in Mechanical Engineering in 1996 from the Massachusetts Institute of Technology and an MS in Mechanical Engineering from the Boston University in 2005. He has worked in the custom automation and defense industries, specializing in multidisciplinary R&D and prototyping. He is currently a Staff Electromechanical Engineer at the Wyss Institute for Biologically Inspired Engineering, involved in the design and prototyping of medical devices, including the mechanical design of the IOTA system.

Conor Walsh is an Assistant Professor of Mechanical and Biomedical Engineering at the Harvard School of Engineering and Applied Sciences. He is also the founder of the Harvard Biodesign Lab, which brings together researchers from the engineering, industrial design, medical, and business communities to develop smart medical devices in collaboration with clinicians. Conor received his BAI and BA Degrees in Mechanical and Manufacturing Engineering from Trinity College in Dublin, Ireland, in 2003, and MS and PhD Degrees in Mechanical Engineering from the Massachusetts Institute of Technology in 2006 and 2010.

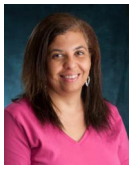

Annette Correia, OT, received a Bachelor's Degree in Science with a major in Occupational Therapy from the University of New England. Annette is an Occupational Therapist with extensive experience in pediatrics and has been at Boston Children's Hospital for 26 years. Areas of interest include hand therapy, sensory integration, constraint, power mobility, prematurity, and custom splinting. Areas of current research include robotics, clinical drug trial for children with Progeria, and pediatric hand transplant. She is certified in the Sensory Integration and Praxis Test (SIPT).

Dr Leia Stirling received BS and MS Degrees in Aeronautical and Astronautical Engineering from the University of Illinois at Urbana-Champaign and a PhD in Aeronautical and Astronautical Engineering from the Massachusetts Institute of Technology in 2003, 2005, and 2008, respectively. From 2008 to 2009, she was a Postdoctoral Research Fellow at Boston Children's Hospital and Harvard Medical School. From 2009 to 2013, she was a Senior Staff Engineer at the Wyss Institute for Biologically Inspired Engineering at Harvard University. Currently, she is an Assistant Professor at the Massachusetts Institute of Technology. Her research interests are in computational dynamics, human-machine interaction, system automation, experimental biomechanics, and quantifying human variability. Dr Leia Stirling is the corresponding author and can be contacted at: leia@mit.edu